Metabolism 168 (2025) 156237



Contents lists available at ScienceDirect

Metabolism

journal homepage: www.journals.elsevier.com/metabolism





Spatial lipidomics reveals sphingolipid metabolism as anti-fibrotic target in the liver

Aleksandra Gruevska [a], Jack Leslie [b], Elena Perpiñán [c], Hannah Maude [a], Amy L. Collins [b], Sophia Johnson [b], Laila Evangelista [a], Eleanor Sabey [a], Jeremy French [d], Steven White [d], John Moir [d], Stuart M. Robinson [d], Wasfi Alrawashdeh [d], Rohan Thakkar [d], Roberta Forlano [a], Pinelopi Manousou [a], Robert Goldin [a], David Carling [e,f], Matthew Hoare [g], Mark Thursz [a], Derek A. Mann [b], Inês Cebola [a], Joram M. Posma [a], Niloufar Safinia [c], Fiona Oakley [b,h], Zoe Hall [a,*]

[a] Department of Metabolism, Digestion and Reproduction, Imperial College London, London, United Kingdom
[b] Newcastle Fibrosis Research Group, Biosciences Institute, University of Newcastle, Newcastle-upon-Tyne, United Kingdom
[c] Department of Inflammation Biology, Institute of Liver Studies, School of Immunology and Microbial Sciences, James Black Centre, King's College London, London, United Kingdom
[d] Department of Hepatobiliary Surgery, Newcastle upon Tyne Hospitals NHS Foundation Trust, Newcastle-upon-Tyne, United Kingdom
[e] MRC Laboratory of Medical Sciences, London, United Kingdom
[f] Institute of Clinical Sciences, Faculty of Medicine, Imperial College London, London, United Kingdom
[g] Early Cancer Institute, University of Cambridge, Cambridge, United Kingdom
[h] FibroFind, Unit 26/27, Baker's Yard, Christon Road, Newcastle upon Tyne, United Kingdom

ARTICLE INFO

Keywords:
Lipid metabolism
Steatotic liver disease
Liver fibrosis
Mass spectrometry imaging
Imaging mass cytometry

ABSTRACT

Background and aims: Steatotic liver disease (SLD), which encompasses various causes of fat accumulation in the liver, is a major cause of liver fibrosis. Understanding the specific mechanisms of lipotoxicity, dysregulated lipid metabolism, and the role of different hepatic cell types involved in fibrogenesis is crucial for therapy development.

Methods: We analysed liver tissue from SLD patients and 3 mouse models. We combined bulk/spatial lipidomics, transcriptomics, imaging mass cytometry (IMC) and analysis of published spatial and single-cell RNA sequencing (scRNA-seq) data to explore the metabolic microenvironment in fibrosis. Pharmacological inhibition of sphingolipid metabolism with myriocin, fumonisin B1, miglustat and D-PDMP was carried out in hepatic stellate cells (HSCs) and human precision cut liver slices (hPCLSs).

Results: Bulk lipidomics revealed increased glycosphingolipids, ether lipids and saturated phosphatidylcholines in fibrotic samples. Spatial lipidomics detected >40 lipid species enriched within fibrotic regions, notably sphingomyelin (SM) 34:1. Using bulk transcriptomics (mouse) and analysis of published spatial transcriptomics data (human) we found that sphingolipid metabolism was also dysregulated in fibrosis at transcriptome level, with increased gene expression for ceramide and glycosphingolipid synthesis. Analysis of human scRNA-seq data showed that sphingolipid-related genes were widely expressed in non-parenchymal cells. By integrating spatial lipidomics with IMC of hepatic cell markers, we found excellent spatial correlation between sphingolipids, such as SM(34:1), and myofibroblasts. Inhibiting sphingolipid metabolism resulted in anti-fibrotic effects in HSCs and hPCLSs.

Conclusions: Our spatial multi-omics approach suggests cell type-specific mechanisms of fibrogenesis involving sphingolipid metabolism. Importantly, sphingolipid metabolic pathways are modifiable targets, which may have potential as an anti-fibrotic therapeutic strategy.

* Corresponding author at: Division of Systems Medicine, Imperial College, Burlington Danes Building, Hammersmith Hospital Campus, Du Cane Road W12 0NN, United Kingdom.
E-mail address: zoe.hall@imperial.ac.uk (Z. Hall).

https://doi.org/10.1016/j.metabol.2025.156237
Received 13 January 2025; Accepted 20 March 2025
Available online 22 March 2025
0026-0495/© 2025 The Authors. Published by Elsevier Inc. This is an open access article under the CC BY license (http://creativecommons.org/licenses/by/4.0/).

1. Introduction

Liver fibrosis is the result of persistent hepatic injury, arising in the context of chronic liver diseases, including steatotic liver disease (SLD) [1]. The incidence of liver fibrosis is rapidly increasing, with the growing prevalence of SLD globally [2]. If unchecked, hepatic fibrosis can progress to severe end-stage liver pathologies such as cirrhosis and hepatocellular carcinoma. Furthermore, fibrosis stage is a key prognostic marker for liver-related outcomes and overall mortality [3].

Fibrosis can be defined as a reversible wound-healing process characterised by excessive production of extracellular matrix (ECM) proteins, where functional hepatic parenchyma is progressively replaced by fibrotic tissue [4]. The molecular and cellular events underlying the development and progression of fibrosis are complex, and both hepatocytes and non-parenchymal cells (NPC) have been implicated [5]. However, the drivers for hepatic fibrosis development are not fully understood and pharmacological treatment remains an unmet need.

Given that in SLD, fibrosis occurs in the context of increased hepatic storage of lipids, it is important to investigate lipid metabolism alterations. Dysregulated fatty acid metabolism, such as imbalances between fatty acid synthesis and breakdown, can result in the accumulation of toxic lipid species that give rise to hepatocellular stress, inflammation and death [6]. Subsequently, the complex interaction between different cell types and their surrounding metabolic microenvironment may link aberrant lipid metabolism with inflammation, fibrosis and the accelerated progression of chronic liver disease [7].

The liver is organised into distinct functional and metabolic regions, with around half the genes showing zonated expression patterns [8]. Moreover, lipid deposition, inflammation and fibrosis progress heterogeneously across tissue during SLD, making whole tissue analyses a substantial approximation. It is therefore critical to employ approaches which retain spatial information to fully characterise and investigate the fibrotic niche [9].

In this study, we analysed liver tissue from patients with chronic SLD and three mouse models of liver fibrosis. To better understand the interplay between dysregulated lipid metabolism and different cell types, we used spatial multi-omics technologies: mass spectrometry imaging (MSI) for spatial lipidomics [10] and imaging mass cytometry (IMC) for highly multiplex localisation of protein markers [11]. Furthermore, we studied the alterations of hepatic gene expression connected to lipid metabolism, to gain insights into the pathogenesis of liver fibrosis at the molecular level. Overall, our findings revealed that sphingolipid dysregulation is accompanied by the altered expression of metabolic genes localised to specific hepatic cell populations within the fibrotic niche. By inhibiting sphingolipid biosynthetic pathways in activated hepatic stellate cells (HSCs) and human precision cut liver slices (hPCLSs), we further demonstrate the potential of sphingolipid metabolism as a promising anti-fibrotic target.

2. Materials and methods

2.1. Human liver tissue samples

Liver tissue was collected from 20 patients with SLD-cirrhosis undergoing liver transplant or resection and 32 control tissue samples from the normal resection margin of patients with colorectal carcinoma metastases to the liver (CRLM) or focal nodular hyperplasia (Table S1). Tissue surplus to clinical requirements was collected at King's College Hospital (REC: 19/LO/0457), Cambridge University Hospitals NHS Foundation Trust (REC: 20/NI/0109) and Imperial College NHS Trust (REC: 19/EE/0301). Clinical diagnoses were performed at individual hospitals. A subset of CRLM patients had incidental metabolic dysfunction-associated steatotic liver disease (MASLD) confirmed by histopathology and centrally scored ($N = 9$; Table S2). A separate cohort of liver biopsies from patients with non-cirrhotic MASLD ($N = 24$; Table S2) was obtained from the Imperial Hepatology and Gastroenterology Biobank (REC 16/SC/0021). All participants provided written informed consent for the use of clinical data and samples for scientific research purposes. This study was approved by the Research Ethics Committee of Imperial College Healthcare Tissue and Biobank, in accordance with both the Declarations of Helsinki and Istanbul.

2.2. Human precision cut liver slices (hPCLSs) and treatment

PCLSs were generated from human liver tissue obtained from normal resection margin surrounding CRLM from patients undergoing surgical resection at the Newcastle-upon-Tyne Freeman Hospital as described before [12]. This study was approved by the Newcastle and North Tyneside Research Ethics Committee and human liver tissue was collected through the CEPA biobank (17/NE/0070) and used subject to patients written and informed consent. hPCLSs were rested in culture for 24 h, then stimulated with 3 ng/mL of transforming growth factor beta-1 (TGFβ-1) and 50 ng/mL of platelet-derived growth factor (PDGF$\beta\beta$), (PeproTech, London, UK) for a further 72 h. hPCLSs were treated with fumonisin B1 (FB-1) (Enzo Life Sciences, Devon, UK), myriocin (63150–10 mg-CAY), and D-PDMP (10005276-10 mg-CAY); both from Cambridge Bioscience, Cambridge, UK. Media was changed daily, and samples were collected for collagen 1A1 ELISA (96 h) or urea assays (supplementary methods).

2.3. Animal studies

C57BL/6J mice (male, age 8–12 weeks) were bred in house or purchased from Envigo (London, UK). Mice were housed in a temperature-controlled facility with 12 h light/dark cycle and received humane care with free access to food and water. All animal studies were approved by the Newcastle Ethical Review Committee and performed under a UK Home Office licence in accordance with the ARRIVE guidelines. Mice were randomly assigned to groups to generate the required numbers based on cage and standardised protocols used to minimise nuisance variables. No animals were excluded for this study. Mice were fed a chow diet (RM3, SDS), unless stated elsewhere.

2.3.1. Bile duct ligation

Mice (12–14 weeks) underwent BDL surgery or a sham procedure. Mice were humanely killed using isoflurane terminal anaesthesia 10 days after surgery when moderate hepatic fibrosis stage is seen [13].

2.3.2. Chronic carbon tetrachloride

Mice (8–10 weeks) underwent bi-weekly intraperitoneal injection of 2 μL/g body weight of carbon tetrachloride (CCl_4): olive oil (1:3 *v*/v) or olive oil for up to 8 weeks. Mice were humanely killed at 8 weeks.

2.3.3. Western diet+CCl_4-injury models

Mice (8–10 weeks) were fed a western diet (WD) containing 21.1 % fat, 41 % sucrose, and 1.25 % cholesterol by weight (TD.120528, Teklad diets, Inotiv, West Lafayette, IN, USA) and sugar water (23.1 g/L D-fructose; F0127 and 18.9 g/L D-glucose; G8270; Sigma-Aldrich, St. Louis, MO, USA) for 12 weeks. WD + CCl_4 injured mice were fed a WD with weekly low dose of intraperitoneal CCl_4 (0.32 μg/g of body weight of CCl_4: olive oil (1:3 *v*/v)) for 20 weeks and then maintained on WD for a further 10 weeks before being humanely killed [14].

2.4. Cell culture and treatment

LX-2 cells (Sigma Aldrich), an immortalized human HSC line [15], were treated with sphingolipid metabolic pathway modulators including: N-Acetyl-D- sphingosine (C2-ceramide, A7191-1MG, Sigma Aldrich), FB-1 (Enzo Life Sciences), myriocin (63150–10 mg-CAY), miglustat (21065-10 mg-CAY) and D-PDMP (10005276-10 mg-CAY); all from Cambridge Bioscience. All treatments were dissolved in DMSO (denoted as vehicle (Veh)), except for FB-1 that was water soluble.

TGFβ-1 (2.5 ng/mL) was used as a positive, pro-fibrogenic challenge that was added as a co-treatment with the inhibitors and/or Veh. Cell viability assay and protein expression analysis by Western blot are detailed in supplementary methods.

2.5. RNA extraction and sequencing

RNA isolation from mouse liver and RNA sequencing methods are described in supplementary methods. Differential gene expression was evaluated using DESeq2 with Benjamini-Hochberg correction [16]. Pathway enrichment analysis was performed using GSEA software v4.0.3 with gene sets (Gene Ontology: Biological Processes) downloaded from MSigDB v7.4 [17,18].

2.6. Analysis of published transcriptomics data

Processed spatial transcriptomics data (median-normalized average gene expression; Visium, 10× Genomics) comparing parenchymal and fibrotic liver regions from 8 patients with cirrhosis were downloaded [19]. Gene lists from metabolic pathways identified in this work were compiled based on the KEGG pathway database [20]. Genes significantly upregulated or downregulated between parenchymal and fibrotic regions were calculated using parametric two-tailed paired Student's *t*-test and applying Benjamini- Hochberg correction for multiple testing. Adjusted *p*-values <0.05 were considered significant. Published single-cell RNA sequencing (scRNA- seq) data from the human Liver Cell Atlas [21] were analysed to look at expression of lipid-related genes in different hepatic cell populations. Full details are provided in the supplementary methods; R scripts available from https://github.com/CebolaLab/Cirrhotic_lipids.

Bulk transcriptomics data from Gene Expression Omnibus (GEO) were analysed. RNA sequencing data on liver biopsies from patients with metabolic-dysfunction associated steatohepatitis (MASH) F0–F1 (N = 34) and MASH F3–F4 (N = 68) were compared (GSE135251; [22]). Additionally, RNA sequencing data on liver from HCC-naïve MASLD patients with fibrosis score F0–F1 (N = 51) and F3–F4 (N = 42) were compared (GSE193066; [23]). Differential gene expression was calculated using DESeq2 with Benjamini-Hochberg correction for multiple testing.

2.7. Bulk lipidomics

Lipidomics analyses were performed using liquid chromatography-mass spectrometry (LC-MS) as previously described [24] and detailed in the supplementary methods.

2.8. Mass spectrometry imaging

Norharmane matrix (Sigma) was applied on tissue cryosections and matrix-assisted laser desorption ionization (MALDI) MSI analysis was performed using AP-MALDI^5 AF ion source (TransMIT, Giessen, Germany) coupled to QExactive Plus mass spectrometer (Thermo Fisher Scientific). Data analysis was carried out using LipostarMSI v2.0 (Mass Analytica, Sant Cugat del Vall'es, Spain). Pixels that mapped to fibrotic and parenchymal tissue regions, in agreement with histology co-registration and confirmed by specialist histopathologist, were set as ROI for subsequent multivariate analysis. Further details in supplementary methods.

2.9. Imaging mass cytometry

Cryosections (10 μm) adjacent to those used for MSI were stained using a 16-antibody cocktail (Table S3) according to manufacturer's instructions. Visualisation and comparison between parenchymal and fibrotic regions was carried out with MCD Viewer software (Standard Biotools). Individual IMC channels and MSI single ion images were co-registered and spatial correlation assessed in MATLAB (MathWorks, Natick, MA, USA) using the Matthews Correlation Coefficient (MCC) [25]. Further details in supplementary methods.

3. Results

3.1. Lipid metabolism is altered in cirrhotic liver from patients with steatotic liver disease

To investigate how lipid metabolic pathways are dysregulated in liver fibrosis, we carried out untargeted lipidomics and multivariate statistical analysis on cirrhotic liver tissue from patients with underlying SLD (N = 20). Patients had either MASLD, alcohol-related liver disease (ALD) or a combination (MetALD). Background liver tissue from patients with CRLM or focal nodular hyperplasia were used as controls (N = 32). We were able to detect hundreds of lipid species, covering a wide range of lipid class including phosphatidylcholine (PC), phosphatidylethanolamine (PE), phosphatidylglycerol (PG), phosphatidylinositol (PI), phosphatidylserine (PS), triacylglyerides (TAG), diacylgclycerides (DAG), ceramides, sphingomyelins (SM), hexosylceramides (HexCer), lactosylceramides (LacCer), trihexosyl- ceramides (Hex3Cer), free fatty acids (FFA), cardiolipins (CL), acylcarnitines (ACar), and lysophosphatidylcholines (LPC).

Patients with SLD-cirrhosis were highly discriminated from control based on their lipid profiles (Fig. 1A; OPLS-DA: $R^2 = 0.84$, $Q^2 = 0.70$, $p = 2.6 \times 10^{-11}$). Importantly, the lipid profiles of the cirrhotic samples were broadly similar across the different aetiologies (Fig. S1). The corresponding S-plot (Fig. 1B) and univariate analysis (Fig. 1C-D) revealed lipids significantly different between SLD-cirrhosis and control. Lipids significantly increased in SLD-cirrhosis included ether lipids, saturated PC, LacCer, Hex3Cer and ACar. On the other hand, we found dramatically decreased TAGs, DAGs, ceramides and LPCs. Interestingly, whilst the total SM abundance was decreased, specific species such as SM(34:1) and SM(34:0) were significantly increased in SLD-cirrhosis compared to control. N-6 and n-3 fatty acids are precursors for pro- and anti-inflammatory lipid mediators, respectively. We noted a dramatic increase in n-6/n-3 ratio in PC and PE for the SLD-cirrhotic group, potentially indicating a pro-inflammatory environment (Fig. 1D). Key findings were confirmed using an independent cohort of non-cirrhotic MASLD patients (F0-F3) as control group (Table S2; Fig. S2).

3.2. Sphingolipid metabolism is dysregulated spatially across fibrotic liver tissue

Advanced fibrosis and cirrhosis arising from SLD in humans tend to form fibrous bands around nodules of parenchyma. To investigate metabolic alterations specifically occurring within fibrotic regions, we used MSI to analyse and visualise the lipidomic changes spatially across liver tissue.

We carried out MSI on a subset of the human SLD-cirrhotic livers (N = 8). Initially, we explored the individual distribution of abundant lipids and found complementary spatial patterns. For example m/z 772.519 corresponding to PC(32:0) [M + K]+, and m/z 770.507 corresponding to PC(32:1) [M + K]+, were mainly distributed within and adjacent to fibrotic regions. On the other hand, m/z 796.523 corresponding to PC (34:2) [M + K] + was mainly located in parenchyma (Fig. 2A).

Next, for each sample we carried out k-means clustering (Fig. 2B) of mass spectral features across all pixels. Using adjacent hematoxylin and eosin (H&E)-stained tissue sections we could associate individual clusters with histological regions, i.e. fibrotic and parenchymal tissue. We defined regions of interest (3 ROIs per cluster per sample) and extracted the mass spectra. Annotated mass spectra from selected ROIs were used to generate an OPLS-DA model (Fig. 2C). We found that the metabolic environment of fibrotic tissue was highly distinct from its surrounding non-fibrotic tissue ($R^2 = 0.96$, $Q^2 = 0.94$, $p < 0.00001$).

We went on to compare the relative intensities of all identified lipids

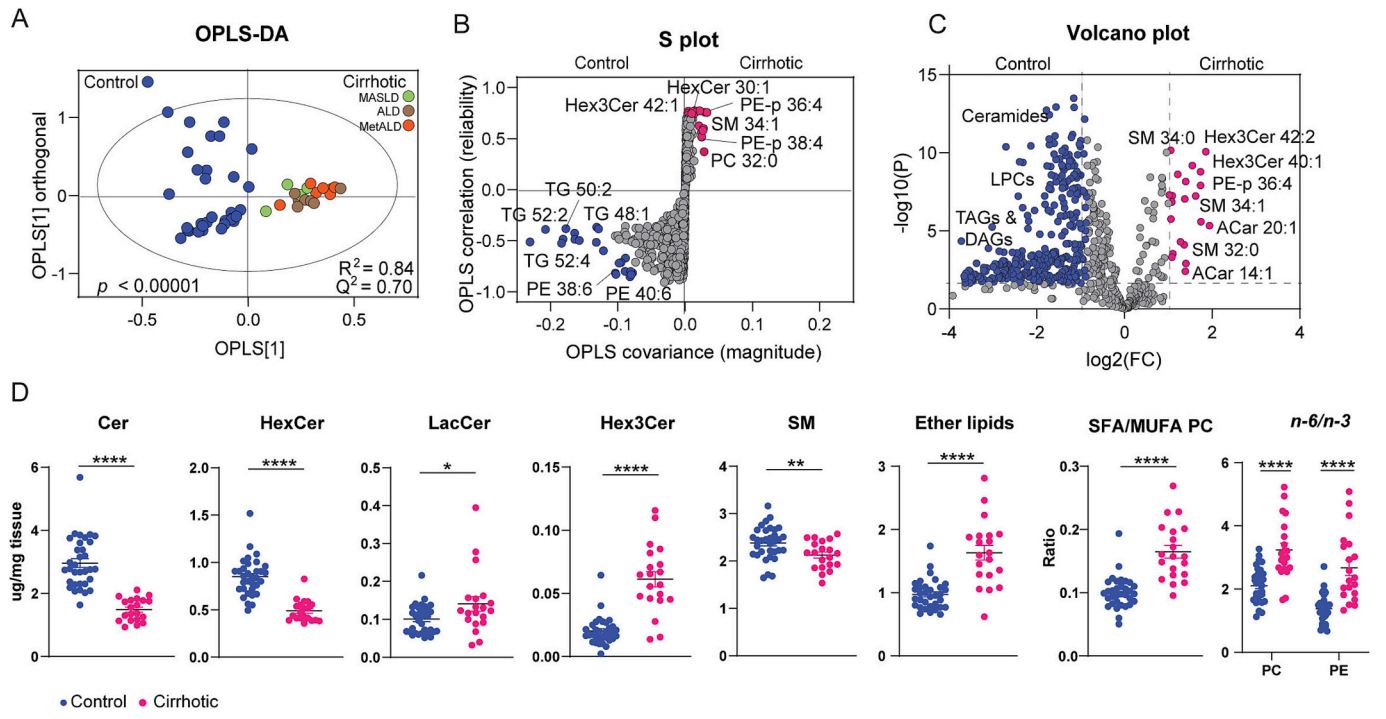


Fig. 1. Human SLD-cirrhotic liver has significantly different lipid signature compared to control. **(A-B)** Hepatic lipid profiles were measured by LC-MS and compared using multivariate analysis. OPLS-DA models and their associated S-plots were constructed to compare SLD-cirrhotic group ($N = 20$) versus control group ($N = 32$). Cirrhotic patients with different aetiologies are shown in different colours. **(C)** Univariate analysis and volcano plots revealed lipid signature is significantly different between groups. **(D)** Bulk tissue lipidomics showed that several lipid classes have altered abundance in cirrhotic liver. Data (mean ± SEM) were analysed using Student's *t*-test: $*p < 0.05$, $**p < 0.01$, $****p < 0.0001$. SFA, saturated fatty acid; MUFA, monounsaturated fatty acid.

in fibrotic versus parenchymal tissue across the different patient samples. More than 40 lipid species were significantly increased in fibrotic tissue (two-tailed *t*-test, *padj* < 0.05, fold change >1.5) and were classified according to lipid class. The major lipid classes enriched in fibrotic regions were ether lipids (including plasmalogens) and sphingolipids (SM, HexCer and CerPE) (Fig. 2D). In contrast, lipid classes enriched in parenchyma included PC, PE and PI. Saturation of PC was also critical, with increased saturated fatty acid-containing PC species detected in fibrotic regions (Fig. 2C-D, Fig. S3A). On the other hand, unsaturated PCs were mainly detected in parenchyma (Fig. 2C-D, Fig. S3B), with the exception of arachidonic acid-containing PCs, e.g. PC(38:4), PC(36:4), which were increased in fibrosis along with a dramatic increase in PC n-6/n-3 fatty acid ratio (Fig. S3C).

We found that SM(34:1) was one of the top increased lipids in human fibrosis (3.8 fold change, *padj* < 0.00001). We plotted SM(34:1) ion intensity across the tissue samples and compared to corresponding adjacent picrosirius red (PSR)-stained tissue sections (Fig. 2E). There was excellent correlation ($r = 0.95$, $p < 0.001$) of SM(34:1) distribution with PSR-stained area (Fig. 2F). To assess whether similar changes in SM (34:1) spatial distribution were found in earlier stages of SLD, we carried out MSI on liver tissue from CRLM patients with incidental MASLD, with varying amounts of fibrosis (F0-F2, $N = 9$). Similar to the cirrhotic samples, SM(34:1) was increased in fibrotic regions (Fig. S4A) and its distribution highly correlated with PSR-stained areas (Fig. S4B). These findings are particularly significant as it indicates that sphingolipid metabolic pathways are also altered in the early stages of fibrosis, when the potential for reversibility is greater.

Finally, we carried out bulk lipidomics on a separate cohort of patients with non-cirrhotic MASLD ($N = 24$, Table S2). We found that SM (34:1), as a proportion of total SM content, increased with fibrosis score (Fig. S4C), however this trend did not reach significance. This highlights the importance of spatial techniques for uncovering fibrotic-specific lipid changes.

3.3. Aberrant lipid metabolism in human disease is recapitulated in mouse models of fibrosis

Preclinical mouse models are widely used to study liver fibrosis. To assess the closeness of such models to human disease in terms of lipid metabolism, we selected 3 well established murine models: bile duct ligation (BDL) [26,27], chronic CCl_4-treatment [28] and a western diet (WD) + CCl_4 model to recapitulate some features of MASLD [14]. Schematic summary of experimental design is shown in Fig. 3A.

Following the challenge, all mice exhibited the respective clinical disease-phenotype – developing inflammation and fibrosis, additionally with steatosis for the WD model (Fig. S5A). To investigate how the lipid metabolic phenotype is altered, we carried out untargeted lipidomics (Fig. 3B). Fibrotic and control samples from each model were significantly differentiated based on their lipid profiles (Fig. 3B). In line with the human data, the fibrotic groups had increased saturated PCs and ether lipids in all models (Fig. S5B). Importantly, we also observed accumulation of sphingolipids (SM and HexCer). Whilst HexCer were more generally increased in fibrotic samples, SM changes were chain dependent. For example, SM(34:1) and SM(42:2) were increased in fibrotic samples whereas SM(40:1) was decreased (Fig. 3C). Next, we looked at the overlap between the significantly altered lipids in the mouse models and human SLD-cirrhosis. Interestingly, common increased lipids included SM(34:1), PC(32:0), HexCer(42:2) and PE(P-36:4), whilst common decreased lipids included several ceramide species (Fig. S5C).

Spatial lipidomics and segmentation by k-means clustering revealed that major lipid classes specifically enriched in murine fibrotic regions included sphingolipids, ether lipids and saturated PC (Fig. S5D). Furthermore, as in human fibrosis, SM(34:1) was identified as a key lipid increased in fibrotic regions relative to parenchyma (Fig. 3D). These findings suggest a strong concordance between the lipid composition of human and mouse fibrosis.

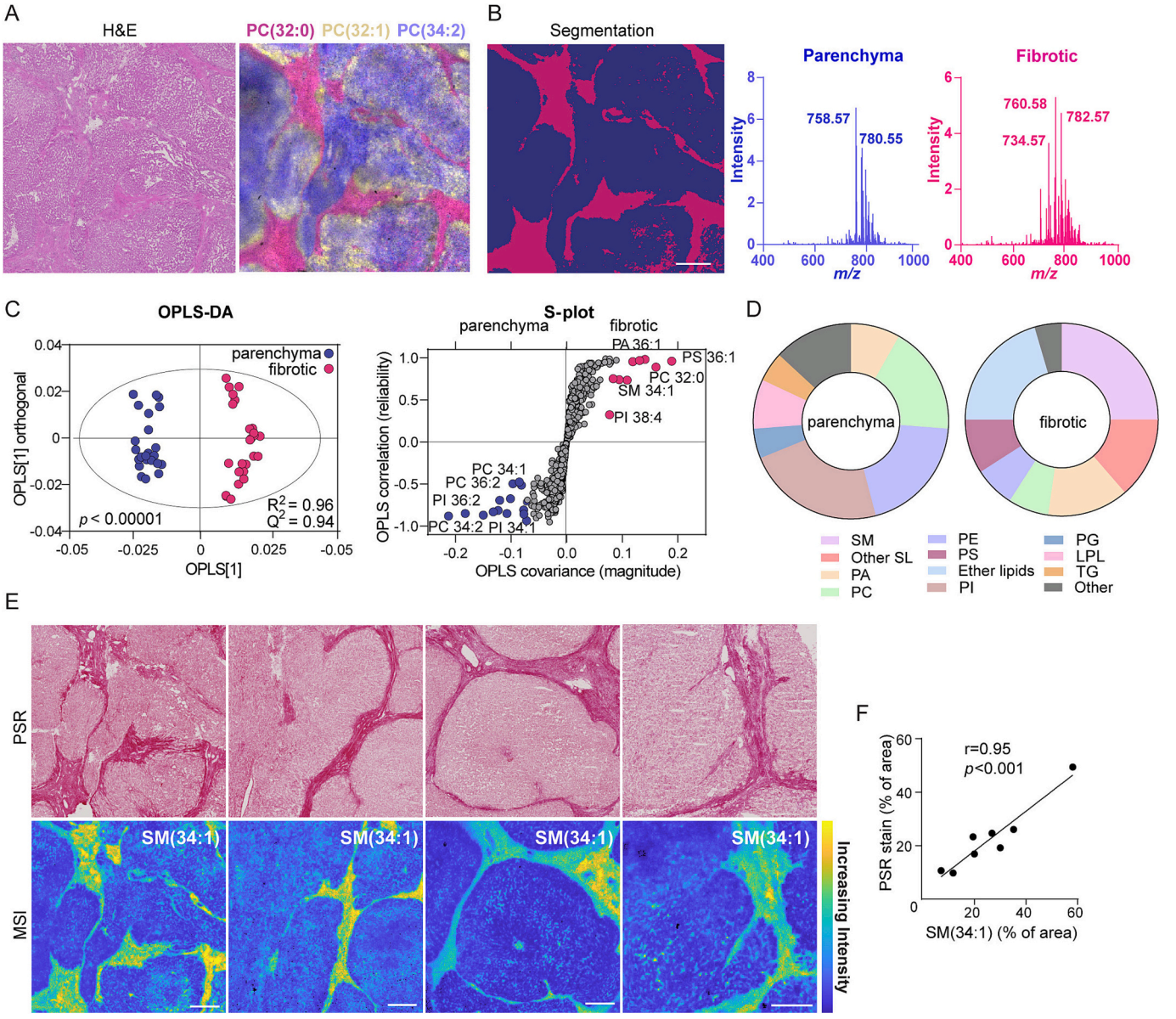


Fig. 2. Lipid metabolism is dysregulated spatially in human steatotic liver disease. **(A)** Spatial lipidomics shows lipid distribution for three lipids: PC(34:2) in blue, PC(32:0) in magenta and PC(32:1) in yellow, with the corresponding H&*E*-stained tissue section. **(B)** Pixels were classified into fibrotic or parenchyma based on their mass spectral profiles. **(C)** Regions of interest (6 per tissue, from 8 different SLD-cirrhotic patients) were selected, corresponding to parenchymal ($N = 24$) and fibrotic ($N = 24$) tissue. OPLS-DA models and their associated S-plots were constructed to compare lipid profiles for parenchyma versus fibrotic ROIs. **(D)** Enriched lipid classes in each tissue region. **(E)** Representative adjacent PSR-stained sections are shown, alongside single-ion intensity images for SM(34:1). Scale bars 500 μm. **(F)** Pearson correlation coefficient between PSR staining and SM(34:1) spatial distribution area. SL, sphingolipids; LPL, lysophospholipids. (For interpretation of the references to colour in this figure legend, the reader is referred to the web version of this article.)

3.4. Transcriptomics reveals changes to lipid metabolism at pathway level in mouse models of fibrosis

To further elucidate which lipid metabolic processes are dysregulated in fibrosis, we explored the transcriptome of the mouse models. Bulk RNA sequencing, followed by pathway enrichment analysis revealed transcriptome- wide changes in all models (Fig. S6A). Normalized enriched score (NES) and false discovery rate (FDR) for all statistically significant pathways are shown in Tables S4–S6. As expected, upregulated genes for all 3 models were enriched for pathways relating to ECM deposition such as: “External encapsulating structure organization”, “Collagen biosynthetic process” and “Collagen fibril organization” (Fig. S6B; Table S7).

In terms of metabolic pathways, there was a significant enrichment in glycosphingolipid (BDL; NES = 1.8, FDR = 0.007, WD + CCl_4; NES = 1.9 FDR = 0.037), ganglioside (BDL; NES = 1.7, FDR = 0.019) and ceramide (BDL; NES = 1.6, FDR = 0.026) metabolic processes in upregulated genes (Tables S4–S7). In the downregulated genes, there was a strong enrichment in pathways pertaining to fatty acid oxidation (BDL and CCl_4 models; NES < -2.8, FDR < 0.00001) and mitochondrial function, including terms: “oxidative phosphorylation” and “mitochondrial respiratory chain complex assembly” (all models; NES < -2.5; FDR < 0.00001; Fig. S6A—B; Tables S4–S7) suggesting decreased lipid catabolism and mitochondrial dysfunction.

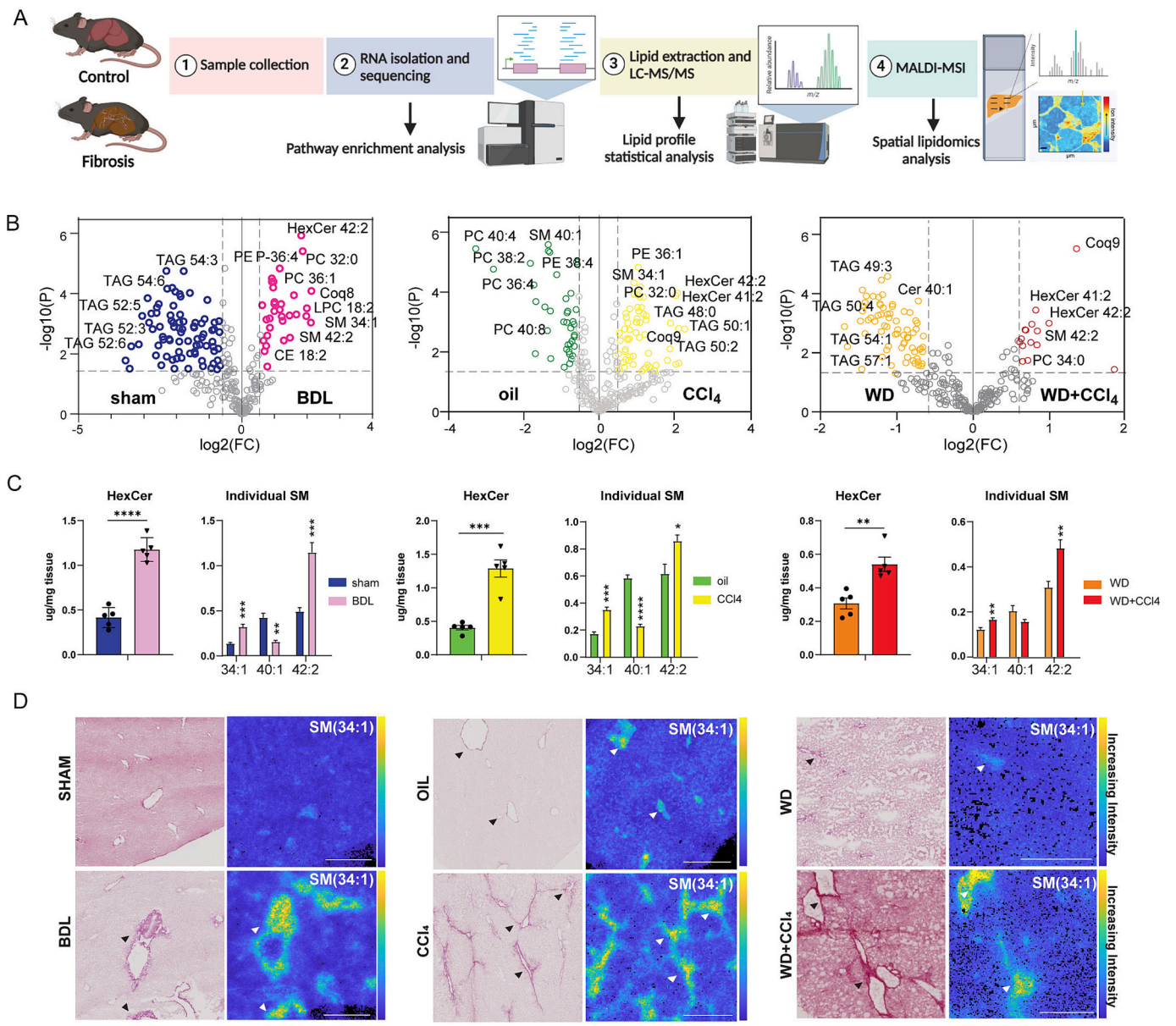


Fig. 3. Lipid metabolism is altered in mouse models of liver fibrosis. **(A)** Schematic summary of experimental design. Hepatic tissue was collected from control (sham, oil, WD) and fibrotic groups (BDL, CCl_4, WD+ CCl_4; $N = 5$ per group. **(B)** Hepatic lipid profiles were measured by LC-MS and compared using univariate analysis. Volcano plots revealed lipid signature is significantly different between fibrotic and control groups. **(C)** Total HexCer and major SM species altered in fibrosis. Data (mean ± SEM) were analysed using Student's *t*-test: *p < 0.05, **$p < 0.01$, ***$p < 0.001$, ****$p < 0.0001$. **(D)** MALDI- MSI showed that SM(34:1) is increased in fibrotic regions of BDL, CCl_4 and WD + CCl_4 groups compared to their respective controls. Adjacent PSR-stained sections are shown, alongside single ion intensity images. Scale bars 500 μm.

3.5. Genes encoding lipid-related metabolic enzymes have altered abundance in fibrosis

From the main lipid classes increased in fibrotic tissue, a list of genes and metabolic pathways were compiled based on the KEGG pathway database [20]. This included ether lipid synthesis, phospholipid remodelling, ceramide metabolism and (glyco)sphingolipid metabolism (Fig. 4A-B; Table S8). First, we assessed whether these genes were differentially expressed in the murine models of fibrosis relative to their respective controls. Next, we investigated whether the genes were differentially expressed between fibrotic and parenchymal liver regions in human cirrhosis, using a recently published spatial transcriptomics dataset [19].

Overall, there was good agreement between differentially expressed genes in the animal models and in human cirrhosis. In particular, there was increased expression of genes related to phospholipid remodelling (*LPCAT1*, *LPCAT2*, *LPCAT4*), synthesis of ether lipids (*FAR1*) and *de novo* synthesis of ceramide (*SPTLC2*, *CERS5/6*, *DEGS1/2*) (Fig. 4A). In addition, gene expression for generation and catabolism of ceramide-1-phosphate (*CERK*, *PLPP2*) and sphingosine-1-phosphate (*SPHK1*, *PLPP2*, *SGPP2*) were increased in mouse models of fibrosis and in human cirrhosis. Several genes involved in glycosphingolipid metabolism had increased expression in fibrosis, including *A4GALT* which is involved in the synthesis of Hex3Cer, a precursor to the globoside series of glycosphingolipids.

We additionally evaluated if any of these genes had altered expression with different fibrosis scores at earlier disease stages. We compared hepatic gene expression from patients with MASLD/MASH with high and low fibrosis scores (F3-F4 versus F0-F1), using published RNAseq datasets GSE193066 and GSE135251. We confirmed that several of the

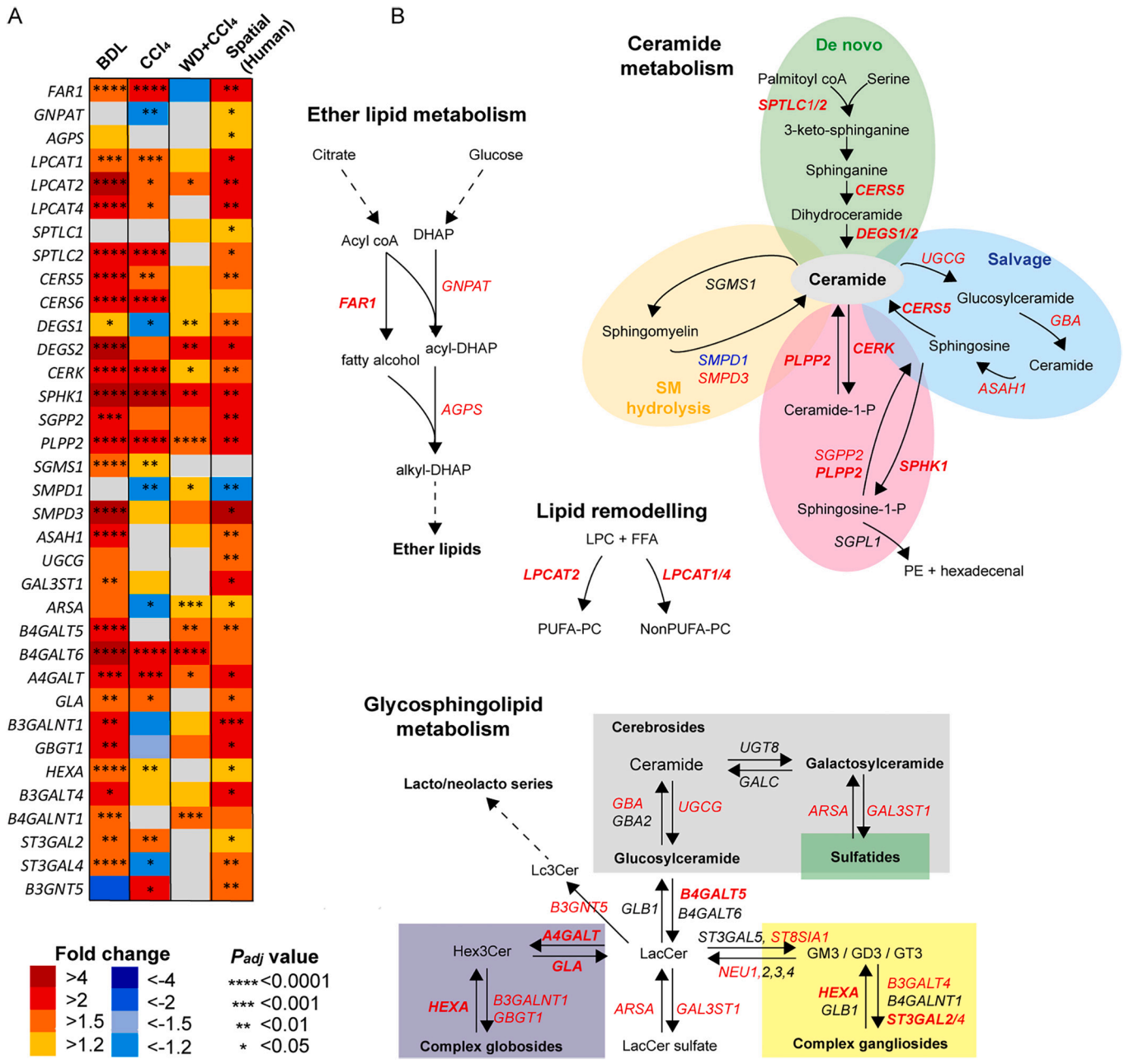


Fig. 4. Genes encoding lipid-related metabolic enzymes have altered abundance in fibrosis. **(A)** Differentially expressed genes from bulk RNAseq data for murine models of fibrosis relative to their respective controls (N = 5 per group) and between fibrotic and parenchymal liver regions in human cirrhosis, from a published spatial transcriptomics dataset [19]; extended in Table S8. **(B)** Metabolic pathways and key genes involved for ether lipid synthesis, phospholipid remodelling, ceramide and glycosphingolipid metabolism. Gene names in red/blue denote significantly increased/decreased expression in human cirrhosis (fibrotic vs parenchyma); name in bold denotes gene expression also significantly altered in the same direction in at least two of the murine datasets. PUFA, polyunsaturated fatty acid; DHAP, dihydroxyacetone phosphate. (For interpretation of the references to colour in this figure legend, the reader is referred to the web version of this article.)

genes involved in lipid remodelling (*LPCAT1/2/4*), ether lipid synthesis (*FAR1*), sphingosine-1-phosphate metabolism (*SPHK1*, *SGPP2*, *PLPP2*) and glycosphingolipid metabolism (*B3GALNT1*, *B4GALNT1*, *B3GNT5*, *GBGT1*) had increased expression in biopsies with higher fibrosis score (Table S8).

To explore the potential origin of accumulated lipids, we examined key genes for lipid synthesis and fatty acid oxidation (Fig. S6C; Table S8). Overall, we found significantly decreased expression for genes involved in mitochondrial (e.g. *ACACB, CPT2, ACADS, ACADM*) and peroxisomal (e.g. *ACOX1/2*) fatty acid oxidation in the mouse and human datasets. On the other hand, several lipogenic genes had increased expression in human fibrosis, including *ACLY* and *SCD5*, with *Scd2* increased in mouse fibrosis. Of further interest was *DGAT2*, with significantly decreased expression in human fibrosis, and in BDL and CCl_4 models. Interestingly, a recent study identified DGAT2 as a key regulator of fat synthesis in the liver [29]. Decreased DGAT2 expression leads to decreased TAG synthesis, reducing steatosis and redirecting DAG to other lipid pathways, which could include ceramide/ sphingolipid synthesis.

3.6. Genes encoding lipid-related metabolic enzymes have cell type-specific expression

The liver hosts a diverse range of resident cell types, all of which

contribute to its functional and metabolic homeostasis. To determine whether expression of key lipid-related genes were cell type-specific, we examined published scRNA-seq data from human liver [21]. This analysis showed that many genes involved in sphingolipid metabolism were widely expressed in NPC, including macrophages and monocytes, stromal cells, endothelial cells and dendritic cells (Fig. 5A, cell clusters annotation in Fig. 5B). For example, *SPTLC2* (which encodes a serine palmitoyltransferase and the first step in ceramide synthesis) was expressed across multiple cell populations, with highest expression in endothelial cells, macrophages, monocytes and monocyte-derived cells (Fig. 5C). *ASAH1* (encoding the acid ceramidase metabolic enzyme) showed expression in multiple immune cell types, with higher levels of expression in macrophages, monocytes and monocyte-derived cells. *SGMS1* (encoding sphingomyelin synthase, which synthesises SM from ceramide) was highly expressed in hepatocytes, endothelial cells, cholangiocytes and stromal cells (Fig. 5C). On the other hand, the sphingolipid-related *UGCG* gene (encoding UDP-glucose ceramide glycosyltransferase, which synthesises glucosylceramide or HexCer) was expressed most highly in plasmacytoid dendritic cells, with expression in endothelial cells, stromal cells and cholangiocytes (Fig. 5C). The individual gene expression of each lipid-related gene in all hepatic cell subpopulations is shown in Fig. S7.

3.7. Integrating spatial lipidomics with imaging mass cytometry links lipids with cell markers

To evaluate the cellular composition of human fibrosis, we further explored the cohort of cirrhotic liver samples analysed by spatial lipidomics (Fig. 2E), by performing IMC on adjacent tissue sections. Our aim was to establish if there was any measurable link between lipid microenvironment in fibrosis and particular cell populations.

To cover the major hepatic cell types, we stained for 16 markers including αSMA, vimentin, CD31, E-Cadherin, cytokeratin (CK) 19, CD45, CD4,

CD68 and others (Table S3). Overall, we found that 11 markers were significantly increased in fibrosis (Fig. S8), whereas 2 were increased in parenchyma. As expected, myofibroblast markers (e.g. αSMA, vimentin), endothelial cell marker (CD31) and leukocytes (CD45) were enriched in the fibrotic regions, whilst epithelial markers E-Cadherin and CK8–18 were specific for parenchymal regions.

Next, we co-registered MSI and IMC images and calculated spatial correlation between lipids and cellular markers (Fig. 6A-B, Fig. S9). Lipids that were found to be increased in fibrotic regions, such as SM (34:1), SM(42:2), PC(32:0), PC(O-34:1), were highly correlated with αSMA, vimentin and collagen (markers for myofibroblasts and ECM; Fig. 6C). There was also good similarity to staining for CD45 and CD3, markers for hematopoietic and T cells, respectively. On the other hand,

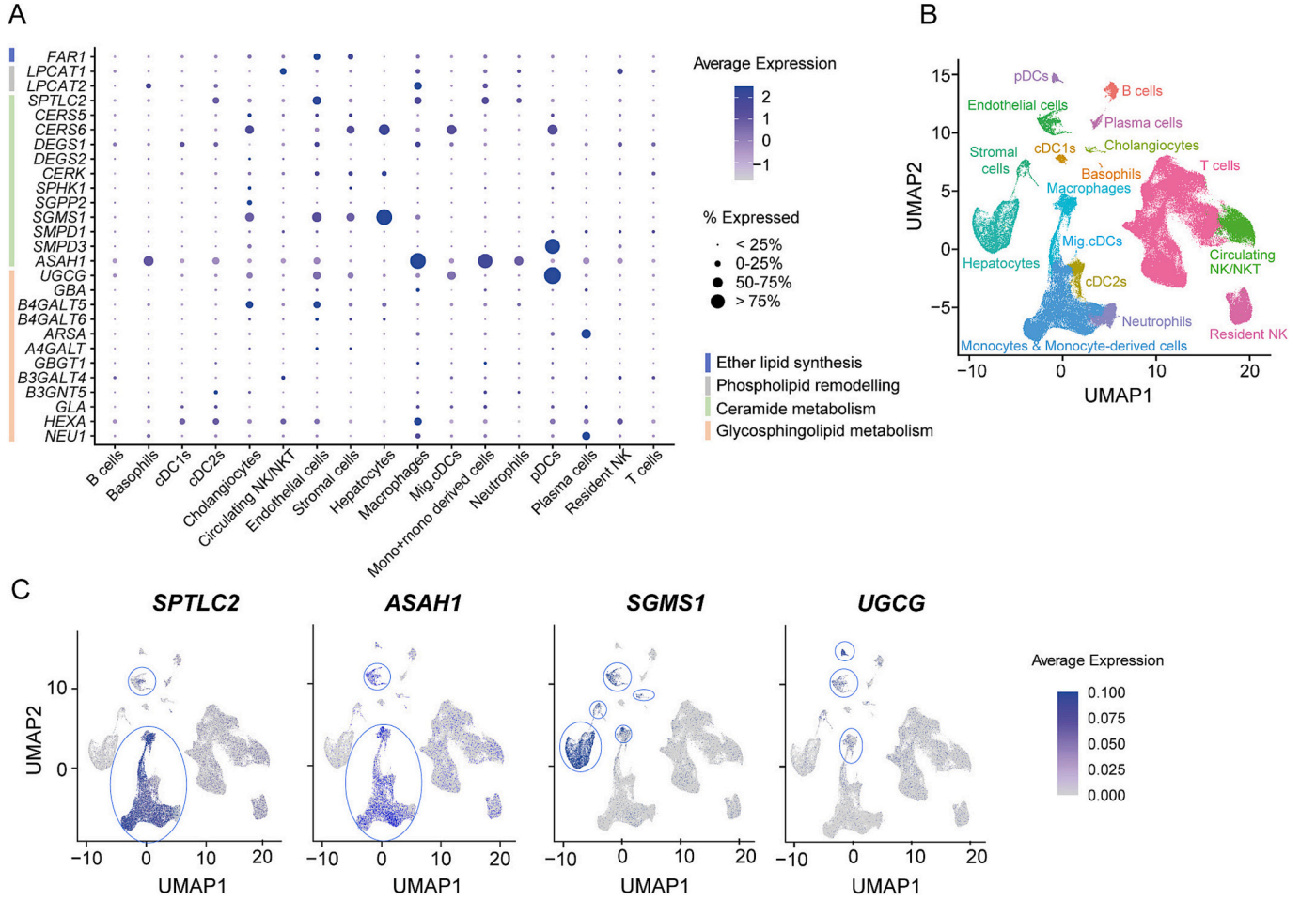


Fig. 5. Genes encoding lipid-related metabolic enzymes have cell type-specific expression. **(A)** Single-cell RNA sequencing (scRNA-seq) data from the human Liver Cell Atlas were analysed for expression of key lipid genes across different cell-type clusters in normal liver. The size of the dots represents the percentage of cells in the cluster with detectable gene expression (counts >0) and the shade represents the average expression across the cluster. Extended list in Fig. S7. **(B)** Uniform Manifold Approximation and Projection (UMAP) highlighting clusters annotated as distinct cell types. **(C)** Expression across cell types for selected genes, shaded by gene expression counts. Major cell types expressing the gene of interest are encircled. cDCs, conventional dendritic cells; pCDs, plasmacytoid dendritic cells; Mig. cDCs, migratory conventional dendritic cells; NK, natural killer cells.

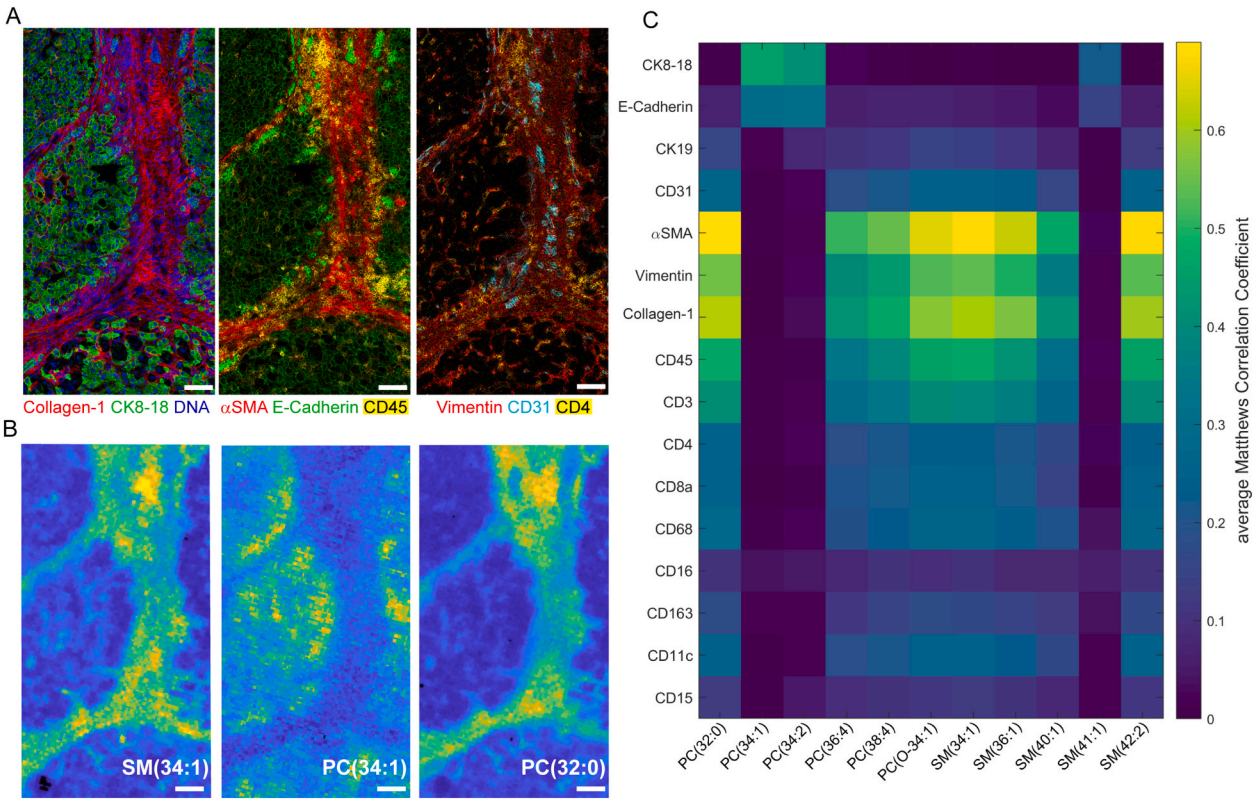


Fig. 6. Integrating spatial lipidomics with imaging mass cytometry of cell markers. Representative images from IMC staining of hepatic cell markers **(A)** and key lipids **(B)** with different spatial distribution in parenchymal and fibrotic tissue regions. **(C)** Heatmap represents the average Matthews Correlation Coefficient between the spatial distribution of lipids and cell markers, across 6 distinct regions of interest and 4 patients. Scale bars 100 μm.

lipids with higher abundance in parenchyma, e.g. PC(34:1), PC(34:2), had closest spatial similarity with epithelial markers such as E-Cadherin and CK8–18 (Fig. 6C).

3.8. Targeting sphingolipid metabolism in activated HSCs and hPCLSs reduces markers of fibrosis

Activated HSCs are the main source of fibrosis in the liver and were enriched in sphingolipid gene expression in our analysis of scRNA-seq data. To investigate if targeting sphingolipid metabolism could reduce fibrosis, we treated LX-2 *in vitro* and hPCLSs *ex vivo* with different inhibitors of sphingolipid pathways, that have been previously described in other studies [30–32] (Fig. 7A). We first analysed cell viability at different time points and treatment concentrations (Fig. S10A). In LX-2, TGFβ-1 was used as pro-fibrotic stimuli and significantly enhanced the expression of pro-fibrotic protein marker αSMA. Treatment with exogenous C2-ceramide decreased αSMA levels, in line with its highly pro-apoptotic effect on the cells (Fig. S10A). Interestingly, inhibition of *de novo* synthesis of ceramides with myriocin (SPT inhibitor) and FB-1 (CerS inhibitor) significantly decreased αSMA protein levels at non-toxic concentrations (Fig. 7B, Fig. S10A). Similarly, targeting the ceramide salvage pathway with glucosylceramide synthase (GCS) inhibitors D-PDMP and miglustat, significantly decreased αSMA protein expression, at concentrations that do not affect cell viability (Fig. 7B, Fig. S10A).

To confirm the efficacy of the inhibitors, we used LC-MS analysis to measure changes in key lipid classes in TGFβ-1-activated LX-2. As expected, the ceramide synthesis inhibitors myriocin and FB-1 dramatically decreased levels of ceramide and downstream species, including HexCer and SM. GCS inhibitors, D-PDMP and miglustat, decreased HexCer and increased ceramide levels, without significantly changing SM (Fig. 7C).

The effects of FB-1, myriocin and D-PDMP treatment were also examined in hPCLSs. hPCLSs are thin, uniform slices of liver tissue used as an *ex vivo* culture model. They retain the liver's 3D structure, physiological ECM composition, and complex cellular interactions, making them valuable for studying hepatic drug metabolism, toxicity, and fibrogenesis. As expected, levels of the fibrillar collagen 1A1 in the hPCLSs culture media were increased with the fibrotic stimuli (TGFβ-1 + PDGF$\beta\beta$) and decreased with the positive control - activin receptor-like kinase 5 inhibitor (Alk5i). Importantly, inhibiting ceramide synthesis with FB-1 treatment significantly reduced collagen 1A1 levels in stimulated hPCLSs (Fig. 7D). Urea levels were not significantly different, suggesting that the treatments at the chosen concentrations did not cause liver toxicity (Fig. S10B). These results show that sphingolipid metabolic pathways are modifiable targets, which may have potential as an anti-fibrotic therapeutic strategy.

4. Discussion

In this study, we have used human samples, mouse models and transcriptomics data to characterise lipid metabolic pathways altered during liver fibrosis. Bulk lipidomic analysis of patients with SLD-related cirrhosis and 3 different mouse models revealed key lipid species with altered abundance in fibrotic samples compared to control. Using spatial lipidomics, we established that these lipids were differentially distributed across fibrotic regions and parenchyma, confirming that lipid metabolism is dysregulated spatially. We further linked specific lipid abundances to their potential regulation via related metabolic gene expression in particular hepatic cell types. We also compared spatial correlation of lipids with cell markers measured using IMC. Taken together this innovative spatial multi-omics approach suggests cell type-specific mechanisms of liver fibrogenesis involving lipid metabolic pathways, including ether lipids, saturation of PC (both discussed

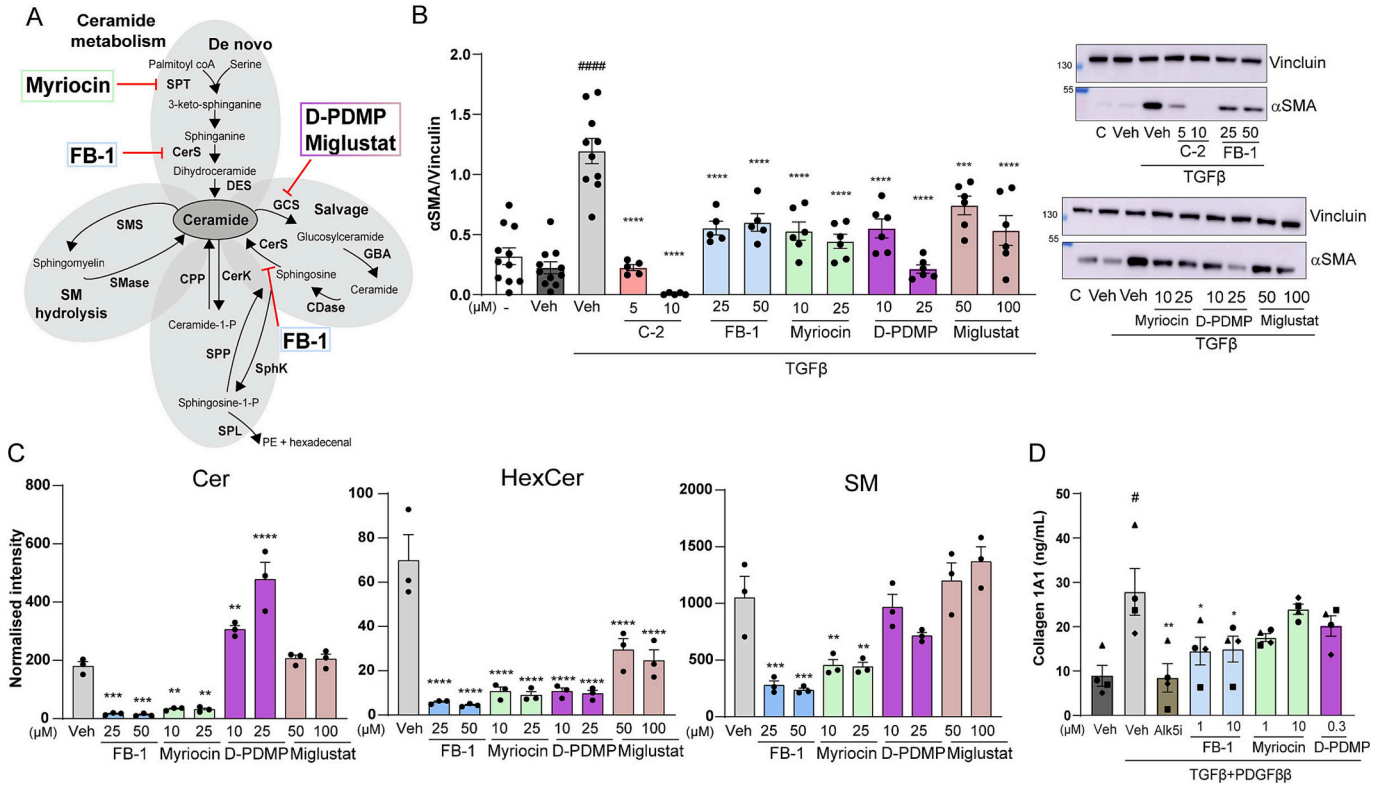


Fig. 7. Targeting sphingolipid metabolism reduces fibrogenic response in activated HSCs and human precision cut liver slices (hPCLSs). **(A)** Schematic view of ceramide metabolism pathway and inhibitors targets. **(B)** LX-2 were co-treated with TGFβ-1 (2.5 ng/mL) and inhibitors of ceramide metabolism or Veh for 72 h. Western blot analysis (N = 5–6) of αSMA protein expression, densitometry and representative images are shown. Data are expressed as a ratio of αSMA signal relative to vinculin signal. **(C)** Lipid profiles of TGFβ-1-activated LX-2, treated with inhibitors for 72 h were analysed by LC-MS (N = 3). **(B—C)** Data (mean ± SEM) were analysed by one-way ANOVA with Bonferroni post-test: $^{**}p < 0.01$, $^{***}p < 0.001$, $^{****}p < 0.0001$ vs Veh + TGFβ-1 or Student's t-test: $\#\#\#\#p < 0.0001$ Veh vs Veh + TGFβ-1. **(D)** Levels of secreted collagen 1A1 measured by ELISA in hPCLSs co-treated with TGFβ-1 (3 ng/mL) and PDGF$\beta\beta$ (50 ng/mL) and inhibitors of ceramide metabolism or Veh for 96 h (N = 4; each donor is shown with different symbol shape). Data (mean ± SEM) were analysed by one-way ANOVA with Bonferroni post-test: $^{*}p < 0.05$,$^{**}p < 0.01$ vs Veh + TGFβ-1 + PDGF$\beta\beta$ or Student's t-test: $\#p < 0.05$ Veh vs Veh + TGFβ-1 + PDGF$\beta\beta$. SPT, serine palmitoyltransferase; CerS, ceramide synthase; DES, dihydroceramide desaturase; GCS, glucosylceramide synthase; GBA, glucocerebrosidase; CDase, ceramidase; CerK, ceramide kinase; CPP, ceramide-1-phosphate phosphatase; SphK, sphingosine kinase; SPP, sphingosine-1-phospate phosphatase; SPL, sphingosine 1-phosphate lyase; SMase, sphingomyelinase; SMS, sphingomyelin synthase; Alk5i, activin receptor-like kinase 5 inhibitor.

further in supplementary) and sphingolipids.

Sphingolipids (particularly ceramide) have been linked to hepatic lipotoxicity, oxidative stress, inflammation, insulin resistance, hepatocyte apoptosis, and fibrosis [33–35]. Previously SM was shown to decrease in plasma/liver from patients with alcohol-related liver fibrosis [36]. Additionally, a multi-omics study revealed that glycosphingolipid metabolism was dysregulated in human MASH [37]. In agreement with these previous studies, we found total SM and HexCer in bulk liver was decreased in human SLD-cirrhosis. However, using spatial lipidomics we discovered specific SM and HexCer species that accumulated within fibrotic regions.

Sphingolipid metabolism was also found to be altered at the transcriptome level in animal models and human fibrosis, with increased gene expression of the enzymes responsible for synthesis of ceramide, increased recycling of bioactive signalling molecules sphingosine-1-phosphate and ceramide-1-phosphate, and increased production of complex glycosphingolipids. Interestingly, analysis of scRNA-seq data revealed that many of the genes involved in these metabolic pathways were widely expressed in NPC, including macrophages and monocytes, stromal, endothelial, and dendritic cells. The distribution of SM species from MSI were compared with staining for ECM and key hepatic cell markers, finding good correlation with collagen, myofibroblast markers and CD45+ cells. To investigate if manipulating lipid metabolism may serve as anti-fibrotic strategy, we targeted sphingolipid pathways in stimulated HSCs and hPCLSs. Our results clearly show that targeting sphingolipid metabolism with inhibitors at non-toxic concentrations exerts an anti-fibrotic effect. Although we have not performed in vivo validation here, other published studies have used sphingolipid metabolic inhibitors in animals to reduce hepatic fibrosis [31,38,39], notably miglustat which mitigated liver fibrosis in CCl_4 mouse model [32]. Miglustat is already an approved drug for treatment of Gaucher disease; drug repurposing is an attractive prospect and warrants further investigation.

Mechanistically, prior research suggests that targeting sphingolipid metabolism can be protective against metabolic diseases by improving mitochondrial function and regulating oxidative stress [40–43]. Our results additionally support a role for sphingolipids in the homeostasis of fibrotic tissue, demonstrating for the first time their spatial distribution in liver fibrosis, and that inhibiting their synthesis in stimulated hPCLSs reduces fibrogenesis. However, further mechanistic studies are needed to fully elucidate the underlying pathways and their implications in liver fibrosis.

Our study has several limitations; in the relatively small and heterogeneous human cohort, there may be potential confounders not taken into account, such as diet, co-morbidities and medication use. It should also be noted that no animal model perfectly recapitulates human disease, and in particular only male mice were used in this study, limiting evaluation of sex-specific effects. Despite these limitations, we identified numerous similarities in altered metabolic features (lipids and gene expression) between mouse models and human samples,

suggesting that much of the metabolic rewiring occurring during liver fibrosis is conserved, including dysregulated sphingolipid metabolism. Higher lipid and gene coverage and improvements in sensitivity and spatial resolution will allow further insights into metabolic states of single cells and how these are altered with SLD progression and fibrosis at the small molecule, protein, and gene expression levels.

5. Conclusion

By integrating different multi-omics and spatial-omics data, we have gained novel insights into metabolic dysregulation in liver fibrosis. In particular, we determined that sphingolipids, such as SM and HexCer, were enriched in fibrotic regions and are linked to non-parenchymal cells. Inhibiting their synthesis exerted an anti-fibrogenic effect in activated HSCs and a human tissue model of fibrosis. Our findings highlight the potential of sphingolipid pathway modulators as a therapeutic approach for fibrogenesis and warrant further studies to explore clinical translatability.

CRediT authorship contribution statement

Aleksandra Gruevska: Writing – review & editing, Writing – original draft, Methodology, Formal analysis, Data curation. **Jack Leslie:** Writing – review & editing, Formal analysis, Data curation. **Elena Perpiñán:** Writing – review & editing, Resources. **Hannah Maude:** Writing – review & editing, Visualization, Methodology, Formal analysis. **Amy L. Collins:** Writing – review & editing, Formal analysis, Data curation. **Sophia Johnson:** Writing – review & editing, Formal analysis, Data curation. **Laila Evangelista:** Writing – review & editing, Formal analysis, Data curation. **Eleanor Sabey:** Writing – review & editing, Formal analysis, Data curation. **Jeremy French:** Resources. **Steven White:** Resources. **John Moir:** Resources. **Stuart M. Robinson:** Resources. **Wasfi Alrawashdeh:** Resources. **Rohan Thakkar:** Resources. **Roberta Forlano:** Writing – review & editing, Resources. **Pinelopi Manousou:** Writing – review & editing, Resources. **Robert Goldin:** Writing – review & editing, Resources, Formal analysis. **David Carling:** Writing – review & editing, Resources. **Matthew Hoare:** Writing – review & editing, Resources. **Mark Thursz:** Writing – review & editing, Resources. **Derek A. Mann:** Writing – review & editing, Resources. **Inês Cebola:** Writing – review & editing, Visualization, Methodology, Formal analysis, Data curation. **Joram M. Posma:** Writing – review & editing, Visualization, Software, Methodology, Formal analysis. **Niloufar Safinia:** Writing – review & editing, Resources. **Fiona Oakley:** Writing – review & editing, Supervision, Resources, Methodology, Formal analysis, Data curation. **Zoe Hall:** Writing – review & editing, Writing – original draft, Visualization, Supervision, Resources, Project administration, Methodology, Funding acquisition, Formal analysis, Data curation, Conceptualization.

Funding

U.K. Medical Research Council (MRC) New Investigator Research Grant MR/W019132/1 (ZH); MRC PhD studentship and program grants MR/K0019494/1 and MR/R023026/1 (JL, DAM, FO); National Institute for Health Research (NIHR) Imperial Biomedical Research Centre (BRC) (ZH, MT); NIHR Newcastle BRC (FO); Sir Henry Dale Fellowship jointly funded by the Wellcome Trust and the Royal Society 224662/Z/21/Z (IC).

Declaration of competing interest

The authors declare the following financial interests/personal relationships which may be considered as potential competing interests:

Fiona Oakley and Derek A. Mann reports a relationship with Fibrofind limited that includes: board membership, consulting or advisory, employment, and equity or stocks. Matthew Hoare reports a relationship with Quotient Therapeutics that includes: consulting or advisory. Matthew Hoare reports a relationship with AstraZeneca that includes: consulting or advisory. Matthew Hoare reports a relationship with Boston Scientific that includes: consulting or advisory. Matthew Hoare reports a relationship with Pfizer that includes: funding grants. Inês Cebola's partner reports a relationship with Ochre Bio that includes: equity or stocks. If there are other authors, they declare that they have no known competing financial interests or personal relationships that could have appeared to influence the work reported in this paper.

Acknowledgements

We thank the MRC Laboratory of Medical Sciences Mass Spectrometry facility team for supporting this work. The NIHR Imperial BRC Genomics Facility contributed to the research results reported within this paper. We thank Professor Zoltan Takats for research support, and the patients who contributed to the study. Presentation: Part of this work was presented at EASL Congress 2023.

Appendix A. Supplementary data

Supplementary data to this article can be found online at https://doi.org/10.1016/j.metabol.2025.156237.

Data availability

Mass spectrometry data is available on MassIVE database (MSV000093530). RNA sequencing data have been deposited in the European Nucleotide Archive (ENA) at EMBL-EBI (PRJEB81328).

References

[1] Hammerich L, Tacke F. Hepatic inflammatory responses in liver fibrosis. Nat Rev Gastroenterol Hepatol 2023;20(10):633–46.
[2] Devarbhavi H, Asrani SK, Arab JP, Nartey YA, Pose E, Kamath PS. Global bur den of liver disease: 2023 update. J Hepatol 2023;79(2):516–37.
[3] Taylor RS, Taylor RJ, Bayliss S, Hagström H, Nasr P, Schattenberg JM, et al. Association between fibrosis stage and outcomes of patients with nonalcoholic fatty liver disease: a systematic review and meta-analysis. Gastroenterology 2020;158(6):1611. 25.e12.
[4] Parola M, Pinzani M. Liver fibrosis: pathophysiology, pathogenetic targets and clinical issues. Mol Asp Med 2019;65:37–55.
[5] Acharya P, Chouhan K, Weiskirchen S, Weiskirchen R. Cellular mechanisms of liver fibrosis. Front Pharmacol 2021;12:671640.
[6] Friedman SL, Neuschwander-Tetri BA, Rinella M, Sanyal AJ. Mechanisms of NAFLD development and therapeutic strategies. Nat Med 2018;24(7):908–22.
[7] Rada P, Gonzalez-Rodrıguez Garcıa-Monzon C, Valverde. Understanding lipotoxicity in NAFLD pathogenesis: is CD36 a key driver? Cell Death Dis 2020;11(9):802.
[8] Halpern KB, Shenhav R, Matcovitch-Natan O, Toth B, Lemze D, Golan M, et al. Single-cell spatial reconstruction reveals global division of labour in the mammalian liver. Nature 2017;542(7641):352–6.
[9] Ramachandran P, Dobie R, Wilson-Kanamori JR, Dora EF, Henderson BEP, Luu NT, et al. Resolving the fibrotic niche of human liver cirrhosis at single-cell level. Nature 2019;575(7783):512–8.
[10] Santos AA, Delgado TC, Marques V, Ramirez-Moncayo C, Alonso C, Vidal-Puig A, et al. Spatial metabolomics and its application in the liver. Hepatology 2024;79(5):1158–79.
[11] Elaldi R, Hemon P, Petti L, Cosson E, Desrues B, Sudaka A, et al. High dimensional imaging mass cytometry panel to visualize the tumor immune microenvironment contexture. Front Immunol 2021;12:666233.
[12] Paish HL, Reed LH, Brown H, Bryan MC, Govaere O, Leslie J, et al. A bioreactor Technology for Modeling Fibrosis in human and rodent precision-cut liver slices. Hepatology 2019;70(4):1377–91.
[13] Gee LMV, Barron-Millar B, Leslie J, Richardson C, Zaki MYW, Luli S, et al. Anticholestatic therapy with obeticholic acid improves short-term memory in bile duct-ligated mice. Am J Pathol 2023;193(1):11–26.
[14] Tsuchida T, Lee YA, Fujiwara N, Ybanez M, Allen B, Martins S, et al. A simple diet- and chemical-induced murine NASH model with rapid progression of steatohepatitis, fibrosis and liver cancer. J Hepatol 2018;69(2):385–95.
[15] Xu L, Hui AY, Albanis E, Arthur MJ, O'Byrne SM, Blaner WS, et al. Human hepatic stellate cell lines, LX-1 and LX-2: new tools for analysis of hepatic fibrosis. Gut 2005;54(1):142–51.
[16] Love MI, Huber W, Anders S. Moderated estimation of fold change and dispersion for RNA-seq data with DESeq2. Genome Biol 2014;15(12):550.

[17] Subramanian A, Tamayo P, Mootha VK, Mukherjee S, Ebert BL, Gillette MA, et al. Gene set enrichment analysis: a knowledge-based approach for interpreting genome-wide expression profiles. Proc Natl Acad Sci 2005;102(43):15545–50.
[18] Liberzon A, Birger C, Thorvaldsdottir H, Ghandi M, Mesirov JP, Tamayo P. The molecular signatures database (MSigDB) hallmark gene set collection. Cell systems 2015;1(6):417–25.
[19] Chung BK, Øgaard J, Reims HM, Karlsen TH, Melum E. Spatial transcriptomics identifies enriched gene expression and cell types in human liver fibrosis. Hepatology Communications 2022;6(9):2538–50.
[20] Kanehisa M, Goto S. KEGG: Kyoto encyclopedia of genes and genomes. Nucleic Acids Res 2000;28(1):27–30.
[21] Guilliams M, Bonnardel J, Haest B, Vanderborght B, Wagner C, Remmerie A, et al. Spatial proteogenomics reveals distinct and evolutionarily conserved hepatic macrophage niches. Cell 2022;185(2):379–96.
[22] Govaere O, Cockell S, Tiniakos D, Queen R, Younes R, Vacca M, et al. Transcriptomic profiling across the nonalcoholic fatty liver disease spectrum reveals gene signatures for steatohepatitis and fibrosis. Sci Transl Med 2020;12: eaba4448.
[23] Fujiwara N, Kubota N, Crouchet E, Koneru B, Marquez CA, Jajoriya AK, et al. Molecular signatures of long-term hepatocellular carcinoma risk in nonalcoholic fatty liver disease. Sci Transl Med 2022;14:eabo4474.
[24] Hall Z, Chiarugi D, Charidemou E, Leslie J, Scott E, Pellegrinet L, et al. Lipid remodeling in hepatocyte proliferation and hepatocellular carcinoma. Hepatology 2021;73(3):1028–44.
[25] Chicco D, Jurman G. The Matthews correlation coefficient (MCC) should replace the ROC AUC as the standard metric for assessing binary classification. BioDataMining 2023;16(1):4.
[26] Kisseleva T. The origin of fibrogenic myofibroblasts in fibrotic liver. Hepatology 2017;65(3):1039–43.
[27] Mederacke I, Hsu CC, Troeger JS, Huebener P, Mu X, Dapito DH, et al. Fate tracing reveals hepatic stellate cells as dominant contributors to liver fibrosis independent of its aetiology. Nat Commun 2013;4(1):2823.
[28] Weber LWD, Boll M, Stampfl A. Hepatotoxicity and mechanism of action of haloalkanes: carbon tetrachloride as a toxicological model. Crit Rev Toxicol 2003; 33(2):105–36.
[29] Rong S, Xia M, Vale G, Wang S, Kim CW, Li S, et al. DGAT2 inhibition blocks SREBP-1 cleavage and improves hepatic steatosis by increasing phosphatidylethanolamine in the ER. Cell Metab 2024;36(3):617–629.e7.
[30] Capolupo L, Khven I, Lederer AR, Mazzeo L, Glousker G, Ho S, et al. Sphingolipids control dermal fibroblast heterogeneity. Science 2022;376(6590):eabh1623.
[31] Martínez L, Torres S, Baulies A, Alarcón-Vila C, Elena M, Fabriàs G, et al. Myristic acid potentiates palmitic acid-induced lipotoxicity and steatohepatitis associated with lipodystrophy by sustaning de novo ceramide synthesis. Oncotarget 2015;6: 41479–96.
[32] Iwanaga T, Chiba T, Nakamura M, Kaneko T, Ao J, Qiang N, et al. Miglustat, a glucosylceramide synthase inhibitor, mitigates liver fibrosis through TGF-/Smad pathway suppression in hepatic stellate cells. Biochem Biophys Res Commun 2023; 642:192–200.
[33] Li Z, Chiang YP, He M, Worgall TS, Zhou H, Jiang XC. Liver sphingomyelin synthase 1 deficiency causes steatosis, steatohepatitis, fibrosis, and tumorigenesis: an effect of glucosylceramide accumulation. iScience 2021 Dec;24(12):103449.
[34] Zhu C, Huai Q, Zhang X, Dai H, Li X, Wang H. Insights into the roles and pathomechanisms of ceramide and sphigosine-1-phosphate in nonalcoholic fatty liver disease. Int J Biol Sci 2023;19(1):311–30.
[35] Ishay Y, Nachman D, Khoury T, Ilan Y. The role of the sphingolipid pathway in liver fibrosis: an emerging new potential target for novel therapies. American Journal of Physiology-Cell Physiology 2020;318(6):C1055–64.
[36] Thiele M, Suvitaival T, Trost K, Kim M, de Zawadzki A, Kjaergaard M, et al. Sphingolipids are depleted in alcohol-related liver fibrosis. Gastroenterology 2023; 164(7):1248–60.
[37] Sen P, Govaere O, Sinioja T, McGlinchey A, Geng D, Ratziu V, et al. Quantitative modeling of human liver reveals dysregulation of glycosphingolipid pathways in nonalcoholic fatty liver disease. iScience 2022;25(9):104949.
[38] Jiang M, Li C, Liu Q, Wang A, Lei M. Inhibiting ceramide synthesis attenuates hepatic steatosis and fibrosis in rats with non-alcoholic fatty liver disease. Front Endocrinol 2019;10:665.
[39] Fucho R, Martínez L, Baulies A, Torres S, Tarrats N, Fernandez A, et al. ASMase regulates autophagy and lysosomal membrane permeabilization and its inhibition prevents early stage non-alcoholic steatohepatitis. J Hepatol 2014;61(5):1126–34.
[40] Yang RX, Pan Q, Liu XL, Zhou D, Xin FZ, Zhao ZH, et al. Therapeutic effect and autophagy regulation of myriocin in nonalcoholic steatohepatitis. Lipids Health Dis 2019;18:179.
[41] Chaurasia B, Tippetts TS, Mayoral Monibas R, Liu J, Li Y, Wang L, et al. Targeting a ceramide double bond improves insulin resistance and hepatic steatosis. Science 2019;365(6451):386–92.
[42] Green CD, Maceyka M, Cowart LA, Spiegel S. Sphingolipids in metabolic disease: the good, the bad, and the unknown. Cell Metab 2021;33(7):1293–306.
[43] Hammerschmidt P, Ostkotte D, Nolte H, Gerl MJ, Jais A, Brunner HL, et al. CerS6-derived sphingolipids interact with Mff and promote mitochondrial fragmentation in obesity. Cell 2019;177(6):1536–52. e23.